Numerical Analysis of the Effect of Injection Pressure Variation on Free Spray and Impaction Spray Characteristics

Park, Kweonha*, Kim, Byung-Hyun

School of Mechanical Systems Engineering, Korea Maritime University

Compression ignition direct injection diesel engines employed a high pressure injection system have been developed as a measure to improve a fuel efficiency and reduce harmful emissions. In order to understand the effects of the pressure variation, many experimental works have been done, however there are many difficulties to get data in engine condition.

This work gives numerical results for the high pressure effects on spray characteristics in wide or limited space with near walls. The gas phase is modelled by Eulerian continuum conservation equations of mass, momentum, energy and fuel vapour fraction. The liquid phase is modelled using the discrete droplet model approach in Lagrangian form and the drop behavior on a wall is calculated with a new droplet-wall interaction model based on the experiments observing individual drops. The droplet distributions, vapour fractions and gas flows are shown in various injection pressure cases. In free spray case which the injection spray has no wall impaction, the spray dispersion and vapour fraction increase and drop sizes decrease with increasing injection pressure. The same phenomena appears more clearly in wall impaction cases.

Key Words : Spray, Injection Pressure, Wall Impaction

1. Introduction

A diesel engine has been increasingly used due to compatibility for high power and low fuel consumption even though considered as a main source of air pollution caused by black smoke and NOx emissions. Recently more application of a diesel engine even for a small car is in prospect as a measure of CO_2 reduction, and its related technologies have been developed in order to improve a fuel consumption and to reduce exhaust emissions. An injection system among those technologies takes an important position and has been developed relating specially to a high pressure injection system electronically controled (Guerrassi and Dupraz, 1998; Nishizawa et al., 1987; Miyaki et al., 1991). The spray characteristics has been studied in constant volume chambers, rapid compression machines, single cylinder engines or multicylinder engines. Bower et al (1992), Nishida et al (1989), Ficarella et al (1997) reported on high pressure fuel spray in a constant volume chamber. Their results showed that the fuel atomization, a tip penetration, fuel mixing with air and evaporation increased with an injection pressure increase. The effects of fuel viscosity and nozzle geometry (Chang and Farrell, 1997), the spray acceleration in the region close to nozzle exit (Hosoya and Obokata, 1992), activation of surrounding air flow and air entrainment (Sasaki et al., 1998) and SMD reduction and a good mixture of the fuel spray near a cavity wall (Minami et al., 1990), studies on combustion characteristics were taken from rapid compression machines or high temperature constant chambers. Kamimoto et al (1987) presented soot formation processes in high pressure injection condition and Verhoeven et al (1998) examined a self ignition site and disper-

* Corresponding Author,
E-mail : khpark@hamara. kmaritime.ac.kr
TEL : +82-51-410-4367 ; **FAX** : +82-51-405-4790
School of Mechanical Systems Engineering, Korea Maritime University, 1 Dongsam-dong, Yeongdo-ku, Pusan, 609-735 Korea. (Manuscript **Received** July 26, 1999; **Revised** November 12, 1999)

sion into spray field. Many investigations were given in engines and their results showed the reduction of self-ignition delay, specific fuel consumption, combustion duration and black smoke instead of increasing NOx (Gyakushi and Takanoto, 1989; Kakegawa et al., 1988; Shundoh et al., 1991; Kato et al., 1989; 1998). Some reports of them gave more details that the combustion characteristics were not improved any more with swirl flow when injection pressure became more than 75MPa (Kakegawa et al., 1988) and there was no black smoke over 150MPa. The above reports showed next; the high pressure injection made the fuel spray just after injection close to the nozzle tip move out rapidly caused by expansion of dissolved compressed gas, and the expansion resulted in fuel atomization. Those high speed sprays moved quickly in company with active gas flows and air entrainments. The tests applied high pressure fuel to high speed small engines showed many sprays impinged on a wall and dispersed with well mixing above the wall especially on cavity wall (Minami et al., 1990). This appearance is completely different from a normal injection case forming a wall fuel film at a low speed fuel impaction on a wall, which means the phenomenon of a fuel impaction on a wall is not the cause of a black smoke any more in a diesel engine with a high pressure injection system. However those experiments upon a high pressure injection were executed in only few cases of injection pressure and had also a limitation of ambient conditions, especially for the spray impinging on a wall. In this study the spray behavior is examined in an engine like high pressure and high temperature gas condition with a wide range of injection pressure from 10MPa to 200MPa for a free spray and also wall impaction spray.

2. Mathematical Model

The gas phase is modelled in terms of the Eulerian conservation equations of mass, momentum, energy and fuel vapour fraction, and turbulent transport is modelled by the $k-\varepsilon$ turbulence model in a form for highly compressed flows. The droplet parcel equations of trajectory, momentum, mass and energy are written in Lagrangian form. The droplet parcel is containing many thousands of drops assumed to have the same size, temperature, velocity components, etc. The actions of the gas phase on the liquid phase are accounted for through the shear terms in the liquid phase momentum equations and the heat transfer terms in the liquid phase energy and fuel mass conservation equations. The efforts of the liquid phase on gas phase is given as sources or sinks in mass, momentum and energy equations in the gas phase. Thus the same basic approach is used as by Watkins (1989), including the non-iterative implicit PISO solution scheme for velocity-pressure linkage. The major difference here is the use of a non-orthogonal grid system, as detailed below.

The gas-phase equations are transformed into general non-orthogonal curvilinear coordinates ξ^i with general tensor notation.

$$\frac{\partial}{\partial t}(\theta\rho\Phi)+\frac{1}{\sqrt{g}}\frac{\partial}{\partial\xi^i}\left(\theta\rho U^i\Phi-\frac{\theta\Gamma_\Phi q_{ij}}{\sqrt{g}}\frac{\partial\Phi}{\partial\xi^i}\right)=\theta S_\Phi+S_\Phi^d \tag{1}$$

The normal flux components U^i to a coordinate surface on which ξ^i is constant is defined by

$$U^i=P_{ij}u^j \tag{2}$$

where u^j are the Cartesian components of a vector field $\vec{V}$, and P_{ij} are the Cartesian components of the area vector which are given as;

$$P_{ij}=\sqrt{g}\frac{\partial\xi^i}{\partial x^j} \tag{3}$$

and Jacobian Determinant $\sqrt{g}=|J|$ is defined by

$$\sqrt{g}=det\,(J_j^i) \tag{4}$$

which is referred to as the infinitesimal volume element at interest point, especially if $\Delta\xi^i=1$, $\sqrt{g}$ is the volume of the cell.

The geometric relations q_{ij} are defined by

$$q_{ij}=\vec{A}^i\cdot\vec{A}^j \tag{5}$$

and $\vec{A}^i$ is the area vector normal to the surface of the control volume.

The source terms are given as follows;

The momentum sources for u^k ($k=1, 2, 3$) are given as

$$\sqrt{g}S_{u^k}=-P_{jk}\frac{\partial P}{\partial\xi^j}+\frac{\partial}{\partial\xi^l}\left(P_{li}\mu_{eff}\frac{P_{jk}}{\sqrt{g}}\frac{\partial u^i}{\partial\xi^j}\right)-\frac{2}{3}P_{jk}\frac{\partial}{\partial\xi^j}\left(\rho k+\mu\frac{1}{\sqrt{g}}\frac{\partial U^m}{\partial\xi^m}\right) \quad (6)$$

The energy source term is

$$\sqrt{g}S_e=-P\frac{\partial U^m}{\partial\xi^m} \quad (7)$$

The kinetic energy source term is

$$\sqrt{g}S_k=\sqrt{g}G_t-\sqrt{g}\rho\varepsilon \quad (8)$$

The kinetic dissipation rate source term is

$$\sqrt{g}S_e=\sqrt{g}\frac{\varepsilon}{k}[C_1G-C_2\rho\varepsilon]+C_3\rho\varepsilon\frac{\partial U^m}{\partial\xi^m} \quad (9)$$

and

$$G=G_t-\frac{2}{3\sqrt{g}}\frac{\partial U^m}{\partial\xi^m}\left(\rho k+\mu_{eff}\frac{1}{\sqrt{g}}\frac{\partial U^m}{\partial\xi^m}\right) \quad (10)$$

$$G_t=\frac{\mu_{eff}}{\sqrt{g^2}}\left[2\left(P_{li}\frac{\partial u^i}{\partial\xi^l}\right)^2+\left(P_{mk}\frac{\partial u^j}{\partial\xi^m}+P_{mj}\frac{\partial u^k}{\partial\xi^m}\right)^2\right] \quad (11)$$

and $C_1=1.44$, $C_2=1.92$, $C_3=-0.373$.

The transformed formulations are discretized by the finite volume manner. Within this process, Euler implicit method is used for the transient term and a hybrid upwind/central difference scheme by Spalding(1980) is used to approximate the convection and diffusion terms.

This wall impaction model is found on experiments conducted on individual droplets(Araki and Moriyama(1982), Jayaratne and Mason (1964), Wachters and Westerling(1966)). These experiments show that the behaviour of droplets after impaction is divided into that normal to and tangential to the wall, and also depends on the Weber number of the drop before impaction.

Wachters and Westerling(1966) have explained the deformation characteristics of a drop impinging on a wall. The shape of the approaching drop is nearly spherical. A short time after the impact the drop undergoes a large deformation and a continuous film spreads out all around a compact central dome. After the end of the spreading of the film, at lower Weber number it shrinks up into a drop again and rises up from the surface and for high Weber number it disintegrates in the film state. However their photographs show that some small drops form and rise up even at high Weber number.

Weber number is defined by

$$We=\frac{\rho_d v_d^2 D_d}{\sigma} \quad (12)$$

where ρ_d is the liquid density, v_d is the drop velocity, D_d is the drop diameter and σ is surface tension.

For the small Weber number $We<2$, the energy loss is accounted for by the velocity relation of the droplet before/after impaction(Jayaratne and Mason(1964))

$$\frac{V_a^2}{V_b^2}=1-0.95\cos^2(\beta) \quad (13)$$

V_a, V_b are the velocities of the drops after and before impaction respectively. Here β is the angle between the approaching drop and the normal to the surface.

In this work the equation is extended for the whole region of Weber number

$$\frac{V_a^2}{V_b^2}=1-k\cos^2(\beta) \quad (14)$$

where the coefficient k is obtained from the relationship between the normal velocity components at arrival and at departure extended from the experimental results of Wachters and Westerling(1966).

On the other hand the velocity component parallel to the surface does not change during the impaction(Wachters and Westerling(1966))

$$\bar{V}_a^t=\bar{V}_b^t \quad (15)$$

where $\bar{V}_a^t$, $\bar{V}_b^t$ are the tangential velocity components of the drops after and before impaction respectively.

For the stable region $We<80$, the velocity component of the drop after impaction normal to the surface is given directly from Eq. (14)

$$(\bar{V}_a^n)_{stable}=-\sqrt{1-k\cos^2(\beta)}\,\bar{V}_b^n \quad (16)$$

In proportion as Weber number increases ($We>80$), the droplet becomes unstable and breaks up into a large number of little droplets. Their velocities after impaction can be modelled by introducing a random instability factor and their direction by random selection. The impacting drop is broken up into many smaller drops. Each

of these new drops could be treated separately. However this would involve an enormous increase in the storage requirements of the computer program. Instead the parcel is broken into two new parcels, and the number of drop into which the impacting drop is broken up is given in terms of the approaching velocity normal to the surface based on Arcoumanis and Chang(1994) and Naber and Farrell(1993). The velocity components of the droplets of the two parcels normal to the surface after impaction are given by

$$(\bar{V}_a^n)^1_{unstable}=(\bar{V}_a^n)^2_{unstable}=(\bar{V}_a^n)_{stable}R_{xx} \quad (17)$$

where $(\bar{V}_a^n)_{stable}$ is the velocity component normal to the surface that is calculated as in the stable region through Eq. (16) and R_{xx} is a random variable uniform in [0, 1].

The velocity components parallel to the surface after impaction are given as

$$(\bar{V}_a^t)^1_{unstable}=\bar{V}_b^t+\bar{V}^t_{scattering} \quad (18)$$

$$(\bar{V}_a^t)^2_{unstable}=\bar{V}_b^t-\bar{V}^t_{scattering} \quad (19)$$

where $\bar{V}^t_{scattering}$ is the scattering velocity which is given randomly as

$$\bar{V}^t_{scattering}=V_{film}P_{xx}\overline{Q_{xx}} \quad (20)$$

P_{xx} is a random variable uniform in [0, 1], $\overline{Q_{xx}}$ is a unit vector in the angle distributed uniformly in [0°, 360°]. The velocity V_{film} of the from of the film around the dome is given by differentiating the equation of the radius(Wachters and Westerling(1966))

$$V_{film}=0.835\left(\frac{3.096}{t^*}-\frac{2t}{(t^*)^2}\right)D_{db} \quad (21)$$

Here t is the time from when the droplet impacts on the surface, D_{db} is the diameter of the droplet before impaction, and the time just after which the dome has disappeared t^* is given as

$$t^*=\frac{D_{db}}{V_b^n} \quad (22)$$

So the film velocity is given by

$$V_{film}=0.835\left(3.096\,V_b^n-\frac{2}{D_{db}}(V_b^n)^2t\right) \quad (23)$$

Here t is given in terms of the value just after the dome disappears, i. e.

$$t=\chi t^*=\chi\frac{D_{db}}{V_b^n} \quad (24)$$

where the coefficient χ will be mainly a function of V_b^n.

Two parcels are selected and arranged to have a scattering velocity component of different sign in order to provide a better stochastic model of the deterministic process described above.

The wall impaction model is summarized as follows;

For We$<$80

$$\bar{V}_a^n=-\alpha\bar{V}_b^n \quad (25)$$

$$\bar{V}_a^t=\bar{V}_b^t \quad (26)$$

$$D_{da}=D_{db} \quad (27)$$

For We$>$80

$$(\bar{V}_a^n)^1=(\bar{V}_a^n)^2=-\alpha\bar{V}_b^nR_{xx} \quad (28)$$

$$(\bar{V}_a^t)^1=\bar{V}_b^t+\bar{V}^t_{scattering} \quad (29)$$

$$(\bar{V}_a^t)^2=\bar{V}_b^t-\bar{V}^t_{scattering} \quad (30)$$

$$D_{da}=C_wD_{db} \quad (31)$$

$$(N_{da})^1=(N_{da})^2=\frac{N_{db}}{2C_w^3} \quad (32)$$

where the subscripts a, b stand for after, before, the superscripts t, n for tangential, normal and 1, 2 for two small parcels after impaction respectively, and $(N_{da})^{1,2}$, N_{db} are the number of drops in the parcel after and before impaction respectively. The energy coefficient α is obtained as;

$$\alpha=\sqrt{1-k\cos^2(\beta)} \quad (33)$$

with β the impinging angle to the normal.

C_w is designed to account for the droplet shattering at high incident Weber number.

The model explained was implemented for a non-orthogonal grid computer code and assessed by Park et al(1996), in which the result of impaction spray have given a good prediction. The results showed a reasonable level of agreement, far superior to other models.

3. Test Conditions

In order to test the injection pressure variation on a diesel engine it is based on the test condition taken by Suzuki et al(1993) to examine the spray and vapor characteristics in high temperature surrounding. An injection pressure range is given from 10MPa to 200MPa at ambient gas temperature 773K and pressure 2.9MPa for free sprays

Table 2 Test cases

	Base	Case 1	Case 2	Case 3	Case 4	Case 5	Case 6
Inj. press.(MPa)	19.6	10	20	30	50	100	200
Nozzle hole dia.(mm)	0.25	0.310	0.249	0.222	0.193	0.161	0.135
Gas press.(MPa)	2.9	2.9	2.9	2.9	2.9	2.9	2.9
Gas temp.(K)	773	773	773	773	773	773	773
Wall Dist.(mm)*	24	24	24	24	24	24	24

* : Only for impaction cases

and wall impaction sprays as given in Table 1. To remove the effect of a fuel injection amount, the injection rates are exactly controlled as following equation.

$$\dot{Q}_{inj} = A \cdot U_{inj} = constant \tag{34}$$

where $\dot{Q}_{inj}$ is an injection rate, A and U_{inj} are a nozzle hole area and an averaged injection velocity at nozzle tip respectively. U_{inj} is given as;

$$U_{inj} = C_d\sqrt{\frac{2(P_{inj}-P_{gas})}{\rho_d}}$$

In this calculation the initial droplet size is obtained from sampling randomly over a discretised spectrum which is symmetric about an average size assumed 30 μm. The drops are broken up with the continuous breakup model of Reitz and Diwaker(1986).

4. Results and Discussion

4.1 Comparison to photos

Figure 1 shows the development of the simulated spray for the base case at 1.2 msec after start of injection and the photograph by Suzuki et al (1993). The predicted spray has a round shape in the spray tip region and small droplets tail diffused up at the vertical section. The shape is fairly similar to the photo and the spray tip penetration and spray width are also in a good match.

Figure 2 gives the shape of fuel vapor fraction by calculation and its photo by (Suzuki et al., 1993) at 1. 2 msec again. The fuel vapor is dispersed widely close to the spray tip and reduced at near to the injection nozzle and little vapor is given in the spray center as shown in the Fig. 2 (b) (Suzuki et al., 1993), and the prediction

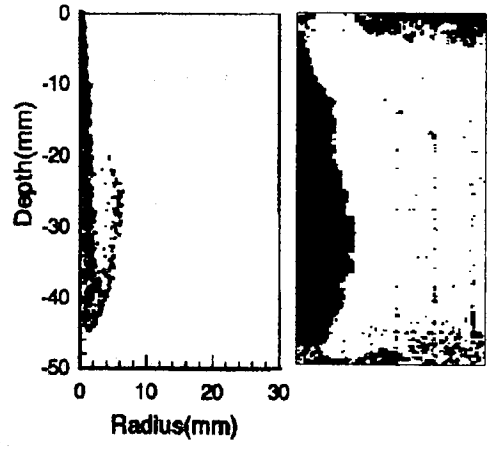

(a) (b)

Fig. 1 Comparison of spray shape
(a) Calculation, (b) Photo of Suzuki [9]

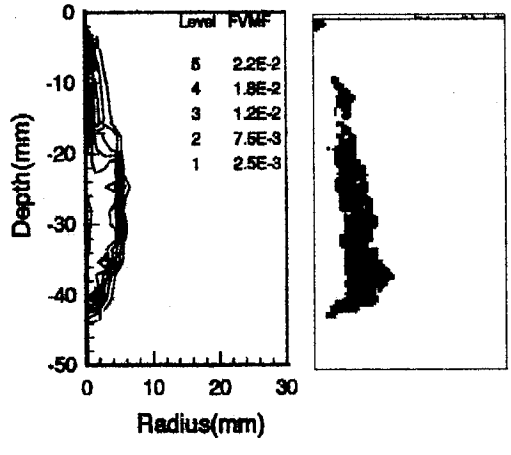

(a) (b)

Fig. 2 Comparison of vapour fraction
(a) Calculation (b) Photo of Suzuki [9]

shows wide dispersion in the middle of the spray depth and more dense vapor in the center of the

spray(radius=0). Nevertheless the overall shapes of the fuel vapor mass fraction given by simulation and experiment are well matched with each other.

4.2 Characteristics of free spray

4.2.1 Spray

Figures 3 and 4 show spray distributions for all the cases and Case 1 and 6 respectively. A dense spray is around on the spray injection axis and does not penetrate to far as shown in Fig. 4(a) for the low pressure injection case, but the high injection case, Fig. 4(b), shows the droplets are far apart each other with a long movement, dispersion through the air and high evaporation caused by the high velocity injection. From Fig. 3 given for all the cases at 0.25, 0.5, 0.75 and 1.00 msec from injection start, the spray movement in the axial direction increases and droplets become smaller as injection pressure increase, specially the spray droplet size reduction appears the tails of the spray returning from the spray end. That phenomenon seems the drops dispersed from the spray axis in the radial direction contact with the surrounding air which has a strong relative velocity and high temperature compared with the region close to spray axis, therefore the droplets become smaller and disappear with quick evaporation.

4.2.2 Vaporized fuel

Fuel vapor mass fractions are shown in Fig. 5 and Fig. 6 for Case 1 and 6 and all the cases

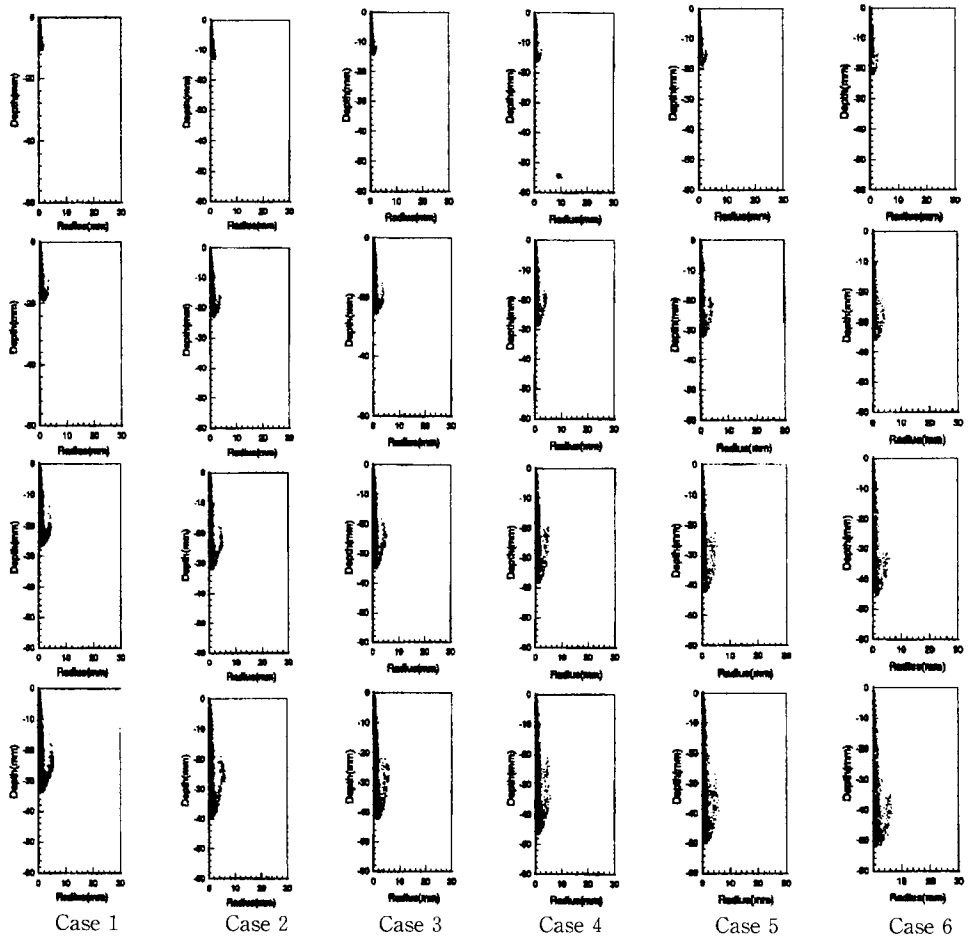

Fig. 3 Comparison of spray development at times of 0.25, 0.5, 0.75, 1.0msec from injection

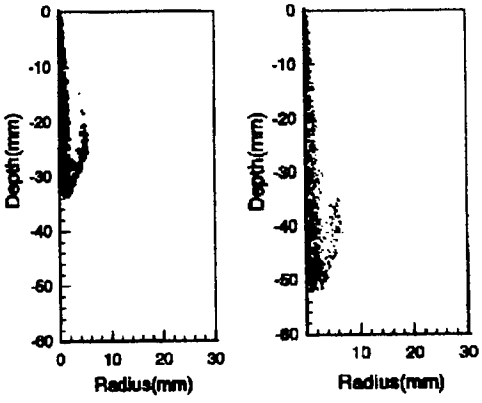

(a) Case 1 (b) Case 6

Fig. 4 Comparison of spray shape

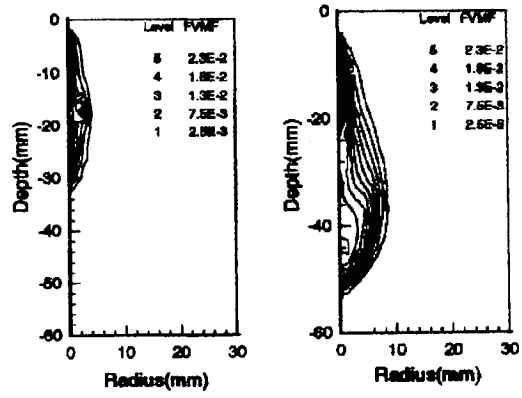

(a) Case 1 (b) Case 6

Fig. 5 Comparison of vapor fraction

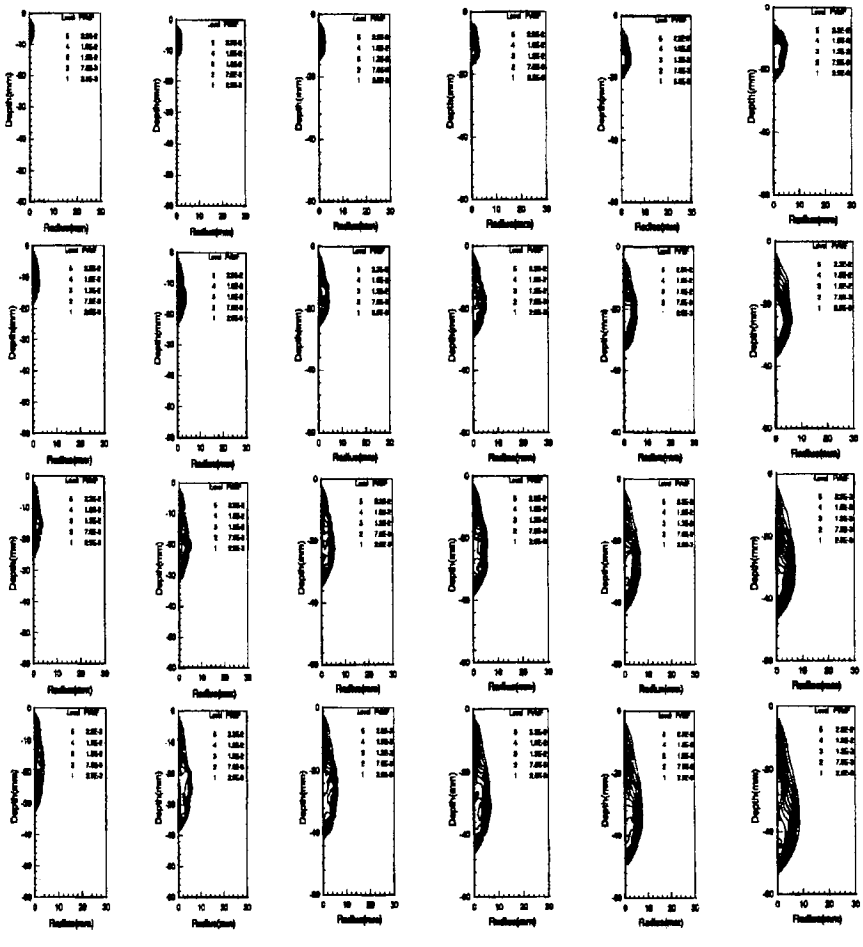

Case 1 Case 2 Case 3 Case 4 Case 5 Case 6

Fig. 6 Comparison of vapour development at times of 0.25, 0.5, 0.75, 1.0msec from injection

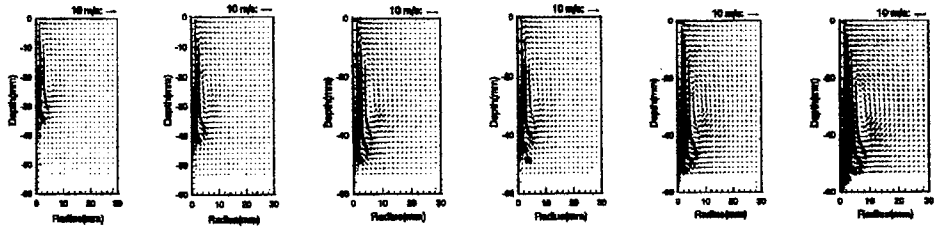

Fig. 7 Comparison of gas flows at 1.0msec from injection start

respectively. Fig. 5(a) for the low injection pressure case shows very narrow contours positioned even inside the spray outline not dispersing, instead of much more wide vapor contours than spray contour as shown in Fig. 5(b) for the high injection case. The high injected fuel vapor is not only around spray region but also much outer, which is considered as the result of evaporation and disappearance of droplets outside of the core area in active interaction with air. Fuel vapors move forward and outward with time flow for all the cases and also with the increase of injection pressure. The effect of the pressure increase appears much clearly at 0.25 msec soon after the injection start, in which the droplets close to nozzle tip have very fast velocities in the high pressure injection case instead of low velocities in the low pressure case on the contrary.

4.2.3 Flow vectors

Fig. 7 shows the gas flow distributions at 1.0 msec from injection start. The flow vector distributions become wider with injection pressure higher. In Case 1 the gas flow develops in just near the spray axis and does not go to far away in both axial and radial directions, but much more active flow and strong air entrainment are shown in Case 6 which makes wide fuel dispersion, well mixing and more vapor.

4.2.4 Spray penetration and width

The tip penetration increase is close to linear variation with time from injection in the low-pressure injection case, but the increasing rate is reduced with time from injection in the high pressure injection case. Not to be questioned, higher the injection pressure, more the spray tip penetrates as shown in Fig. 8.

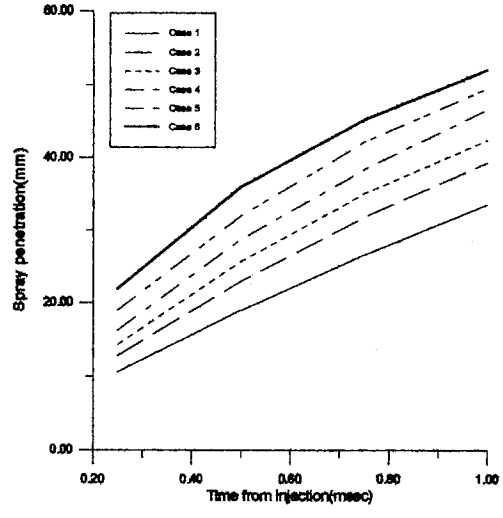

Fig. 8 Comparison of spray penetration

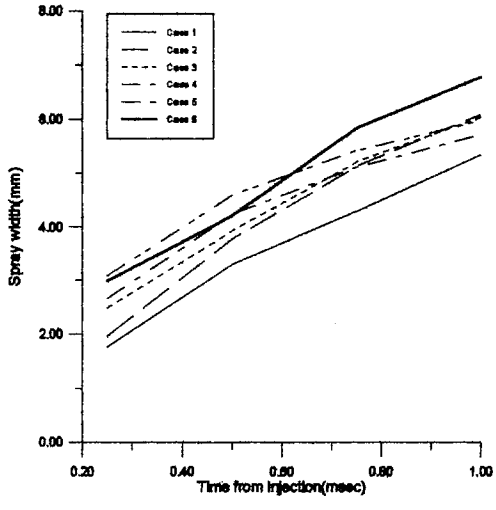

Fig. 9 Comparison of spray width

Comparison of spray width is shown in Fig. 9. The width also increases with increasing time

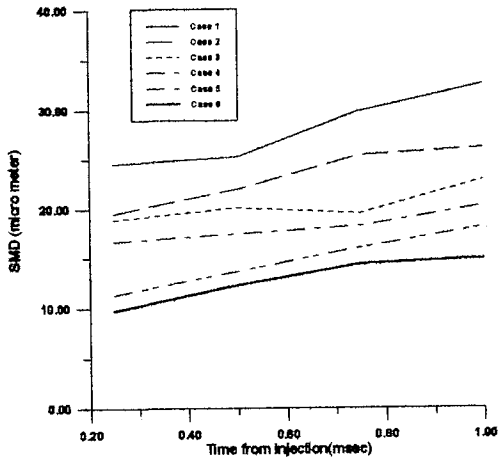

Fig. 10 Comparison of SMD

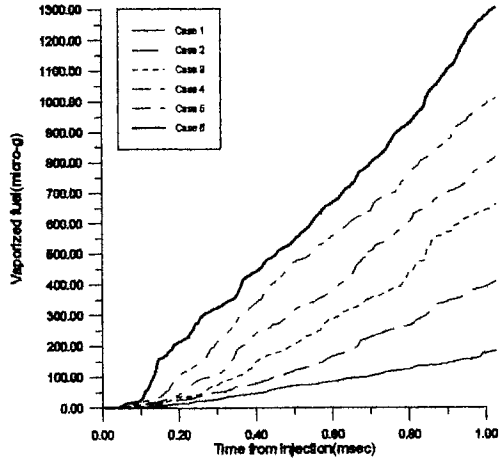

Fig. 11 Comparison of vaporized fuel

from injection, but does not increase with increasing injection pressure. The dispersion widths in radial direction are mixed up with each other after 0.5 msec from injection start except Case 1, and the width in Case 6 is less than in Case 4 even in early time from injection. This non-linearity is considered as the result of evaporation level depended on fuel mixing with air.

4.2.5 Droplet size and fuel vapor

0.25 msec soon after injection start the average drop size is reduced quickly. The Sauter Mean Diameters are 25μm in Case 1 and less than 10 μm in Case 6, which are the reduced sizes from the initial condition 30μm, then the droplets become bigger a little with time increase by coalescence between droplets which is shown in Fig. 10. The atomization in early time form injection depends much on an injection velocity, after that the average droplet sizes vary with time in similar pattern independently of an injection pressure.

Figure 11 shows vaporized fuels. The fuel vapor also increases with increasing injection pressure, specially in early time from injection much more vaporizing appears in the high injection pressure case than in the low injection pressure.

The results above discussed for the free spray are shown in Fig. 12 at 1.0 msec from injection start. The spray tip penetration and the vaporized fuel increase and the drop size decreases with

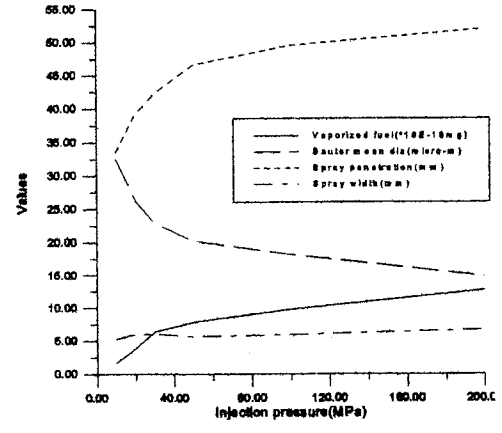

Fig. 12 Spray characteristics vs. inj. pressure

increasing injection pressure. The variations are very dependable in low injection pressure region less than 100MPa, but the effect of pressure increase on spray characteristics is reduced in a high pressure region. The spray width does not give any relations with pressure variation.

4.3 Characteristics of wall impaction spray

4.3.1 Spray

Figure 13 shows spray distributions at 1.5 msec from injection start for Case 1 and Case 6 with the spray impacting on a wall at 24 mm distant from nozzle tip, and Fig. 14 shows wall spray shapes at 0.25, 0.5, 0.75, 1.0, 1.25, 1.5 msec for all the cases. In the low injection case the spray

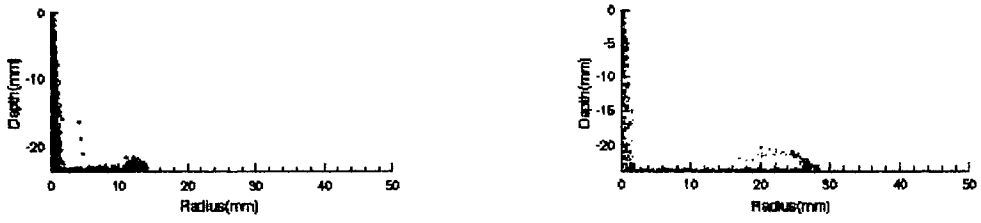

(a) Case 1 (b) Case 6

Fig. 13 Comparison of spray shape

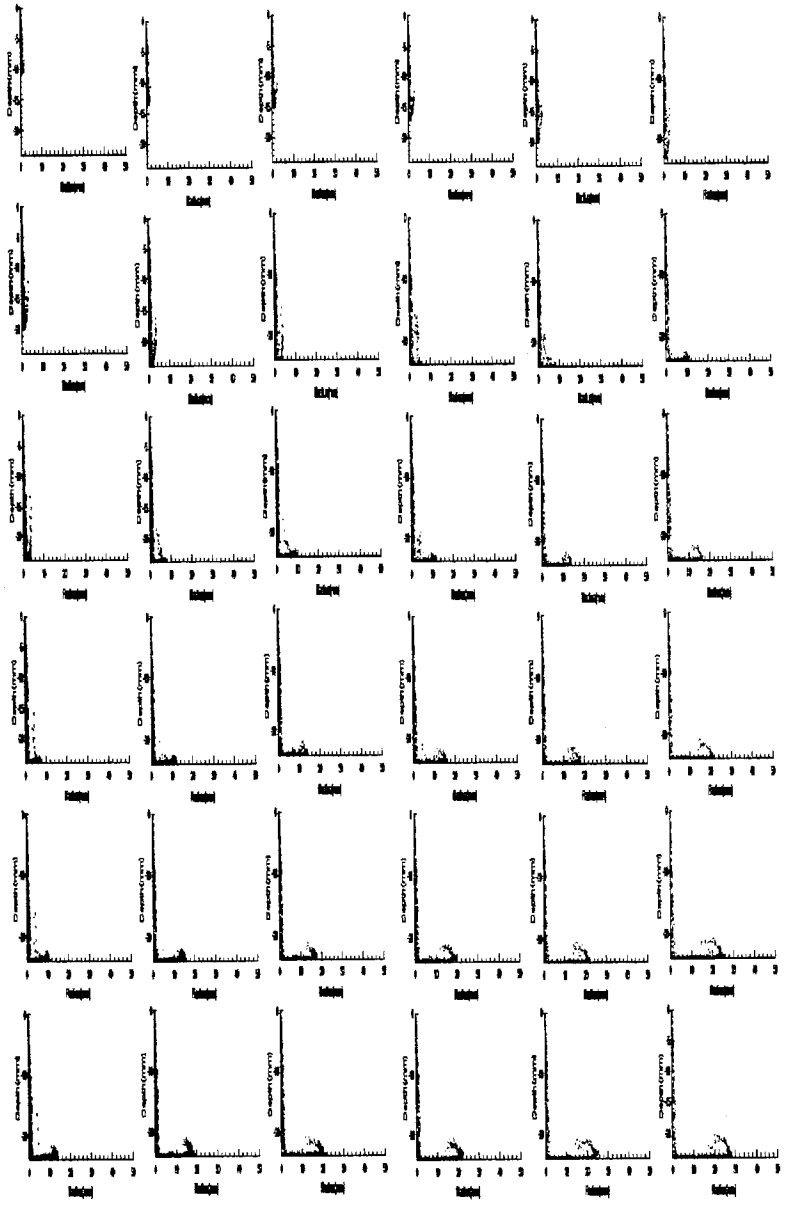

(a) Case 1 (b) Case 2 (c) Case 3 (d) Case 4 (e) Case 5 (f) Case 6

Fig. 14 Comparison of spray shape

moves down to the wall slowly and the spray after impacting on a wall moves out slowly again. So the dense spray stays close to injection spray axis and just on the wall, which allows many chances of drop-drop coalescence. Instead the spray goes down fast and moves out quickly after impacting on a wall in the high injection pressure. Therefore the drops are in distance each other on the wall and form a wide dispersion on the end of the wall spray. Again many small drops appear over the wall spray and specially much smaller drops are in the tail apart from impaction wall in the high pressure case. That says the drops after impacting on a wall with high normal speed are broken up into many smaller drops and move away quickly which removes the chance of drop-drop coalescence making drop size bigger.

4.3.2 Vaporized fuel

Figure 15 shows vapor contour at 0.25 to 1.5 msec for Case 1 and 6. At 0.25 msec the vapor remains just close to spray axis near injection nozzle tip in Case 1, instead of much wider dispersion caused by active gas flow out near the impaction wall. After spray impacting on a wall, the fuel vapor disperses much rather above the wall in the high injection case.

4.3.3 Flow vectors

The main body of the gas flow follows the spray path from injection nozzle to the wall and outward on the wall. At wall jet region near the position where spray impacts, the outward strong flow is shown right upon the wall. The strong outward flow removes the gas from the region and forms a low pressure area which sucks in air

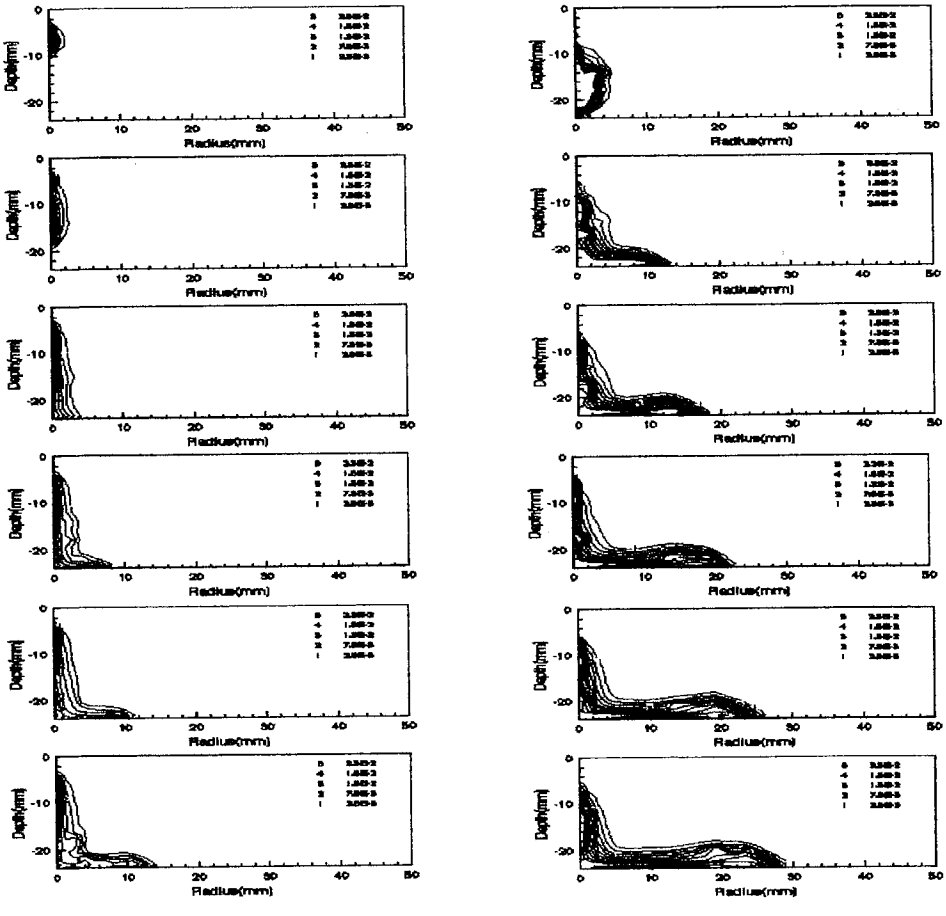

Fig. 15 Comparison of vapour fraction

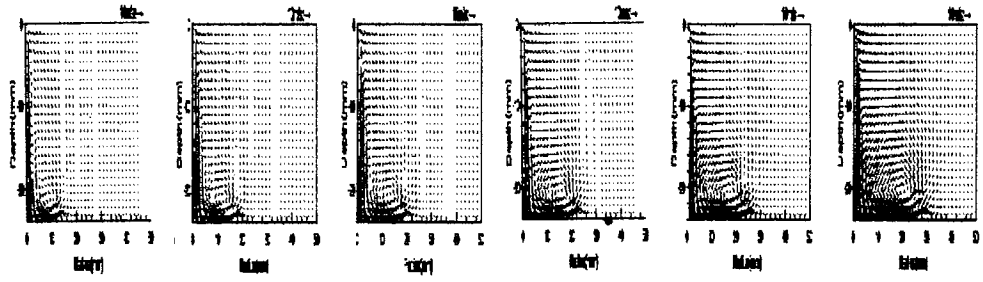

(a) Case 1 (b) Case 2 (c) Case 3 (d) Case 4 (e) Case 5 (f) Case 6

Fig. 16 Comparison of flow vectors from Case 1 to Case 6

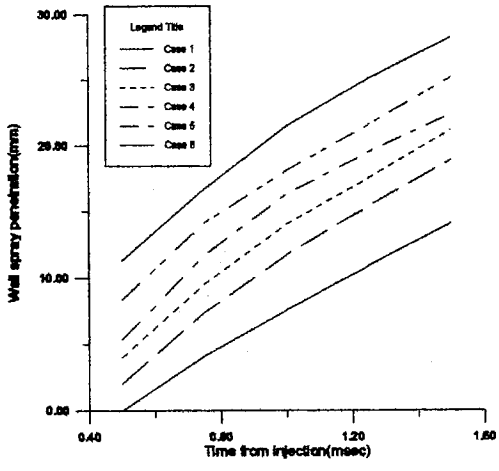

Fig. 17 Comparison of wall spray penetration

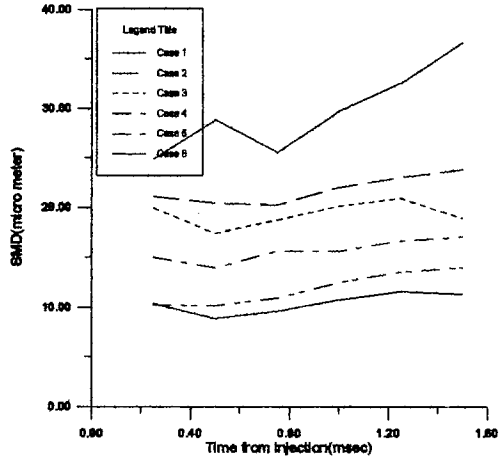

Fig. 18 Comparison of SMD

from surrounding. Therefore the gas flow impacting on a wall moves out strongly and at the same time, the gas returns from the region above the wall jet flow. The flow moving out from the jet region forms a vortex region on the wall spray head. The gas flow does not go out any further by air resistance and turns up and goes back. The higher the injection pressure is the more clear and strong that phenomenon, which is shown in Fig. 16.

4.4.4 Wall spray penetration

The wall spray penetrations are shown in Fig. 17. The spray penetrates further following on the wall with time and pressure increase. The penetration rates are similar to each other but the spray of the high pressure injection case reaches on the wall much earlier which forms more wide spray dispersion.

4.4.5 Drop size and vaporized fuel

Figure 18 and 19 show Sauter mean diameter and amount of vaporized fuel with time increase for all the cases. With pressure increase drops disperse widely which reduces the chance of drop-drop interaction, at the same time the evaporating is accelerated with increasing gas flow intensity of surrounding air. As the result it follows that SMD decreases down to $10\mu m$ with increasing pressure up to 200 MPa. The mean droplet size reduces soon after impacting then increases with time increase, which means the drops impacting on a wall break up into smaller drops, then the drops form thick region just on the wall and become bigger with drop-drop coagulation. Specially the effect is much rather in the low pressure injection case, Case 1, so the averaged drop size rises steeply by the above effect after wall impaction, while the size stays down in the high pressure injection case. The vaporized fuel increases with

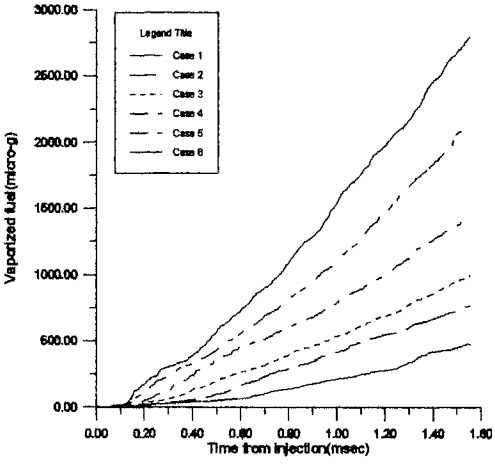

Fig. 19 Comparison of vaporized fuel

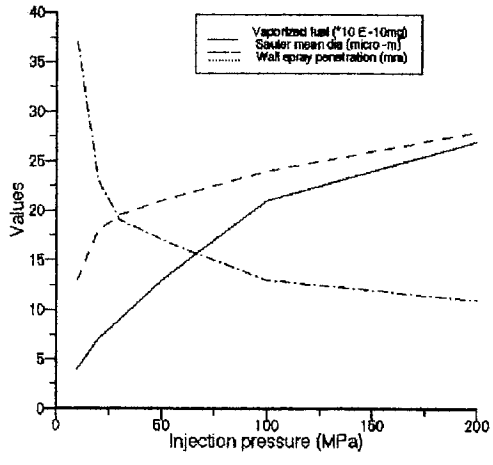

Fig. 20 Spray characteristics vs. inj. pressure

the injection pressure increase and with time increase. Its rate becomes higher with pressure increase as well.

Figure 20 shows the wall spray penetration, Sauter mean diameter and vaporized fuel at 1.5 msec from injection start. The spray penetration and vaporized fuel increase and drop size decreases with the injection pressure increase like in the free spray case. As an important phenomenon, the droplet size of wall impaction case becomes bigger than that of the free spray case in the low pressure injection case, Case 1, instead of smaller in the high pressure case, Case 6. That says the spray impinging on a wall gives a bad effect in a low pressure injection case caused by forming fuel film, on the contrary the wall impaction gives a good effect in a high pressure injection case. Another important factor may be that the effect of pressure increase on a wall spray is reduced with injection pressure increase like that of the free spray in a high pressure region over 100MPa.

5. Conclusion

From the above results, the effects of the injection pressure increase on a free spray are given as;

■ In the low injection pressure case the spray injected with low velocity stays densely in the region just close to the spray axis and is not diffused, which results in generating bigger drops with drop-drop coalescence.

■ In the high injection pressure case the drops distribute widely and the chance of drop-drop collision is reduced, then the drops become smaller with high evaporation caused by high relative velocity between the drops and the gas.

■ Spray tip penetration and vaporized fuel increase and SMD reduces with the increase of injection pressure but spray width has not relation to the injection pressure variation.

The effects of the injection pressure increase on a wall impaction spray are;

■ In the low injection pressure case the spray is again densely near the spray axis and near the wall and then forms bigger drops.

■ In the high injection pressure case the drops break up into much smaller drops and disperse widely by the high speed impaction on a wall. The broken drops are distributed widely and result in smaller drops and more vaporized fuel.

■ After impacting, the drops become bigger with time increase by the drop-drop coagulation effect near wall. The effect is much rather in the low pressure injection case, Case 1, so the averaged drop size(SMD) curve rises steeply, while the curve stays down in the high pressure injection case.

■ Wall spray penetration and vaporized fuel increase and SMD reduces with injection pressure increase.

High pressure injection system improves the

spray characteristics of both free spray and wall spray and might result in improving the performance of diesel engines. However the effect of the increase of injection pressure is reduced in the high injection pressure region over 100MPa, therefore the injection pressure must be chosen with considering total energy concept including the cost for a high pressure injection system.

References

Guerrassi, N. and Dupraz, P., 1998, "A Common Rail Injection System for High Speed direct Injection Diesel Engines," *SAE* paper 980803.

Nishizawa, K., *et al*, 1987, "A New Concept of Diesel Fuel Injection Timing and Injection Rate Control System," *SAE* paper 870434.

Miyaki, M., *et al*, 1991, "Development of New Electronically Controlled Fuel Injection System ECD-U2 for Diesel Engines," *SAE* paper 910252.

Nishida, M., *et al*, 1992, "Observation of High Pressure Fuel Spray with Laser Light Sheet Method," *SAE* paper 920459.

Bower, G. R. and Foster, D. E., 1989, "Investigation of the Characteristics of a High Pressure Injector," *SAE* 892101.

Ficarella, A., Laforgia, D., Starace, G. and Damiani, V., 1997, "Experimental Investigation of the Sprays of an Axi-Symmetric Nozzle of a Common-Rail High Pressure Electro-Injector," *SAE* 970054.

Chang, C. T. and Farrell, P. V., 1997, "A Study on the Effects of Fuel Viscosity and Nozzle Geometry on High Injection Pressure Diesel Spray Characteristics," *SAE* 970352.

Hosoya, H. and Obokata, T., 1992, "Flow Characteristics of High-Speed Spray and Entrainment Air," *JSAE* Vol. 58, No. 548, pp. 270~276.

Sasaki, S., Akagawa, H. and Tsujimura, K., 1998, "A Study on Surrounding Air Flow Induced by Diesel Sprays," *SAE* paper 980805.

Minami, T., Yamaguchi, I., Shintani, M., Tsujimura, K. and Suzuki, T., 1990 "Analysis of Fuel Spray Characteristics and Comustion Phenomena Under High Pressure Fuel Injection," *SAE* 900438.

Kamimoto, T., Yokota, H. and Kobayashi, H., 1987, "Effect of High Pressure Injection on Soot Formation Processess in a Rapid Compression Machine to Simulate Diesel Flames," *Transaction of the SAE*, Vol. 96, Sect. 4, pp. 783~791.

Verhoeven, D., Vanhemelryck, J-L. and Baritaud, T., 1998, "Macroscopic and Ignition Characteristics of High-Pressure Sprays of Single -Component Fuels," *SAE* 981069.

Gyakushi, N. and Takamoto, Y., 1989, "Controlling Factors of Comustion in a D. I. Diesel Engines(ignition delay)," *JSAE*, Vol. 55, No. 519, pp. 3601~3605.

Kakegawa, T., Suzuki, T., Tsujimura, K. and Shimoda, M., 1988, "A Study on Combustion of High Pressure Fuel Injection for Direct Injection Diesel Engine," *SAE* 880422.

Shundoh, S., Kakegawa, T., Tsujimura, K. and Kobayashi, S., 1991, "The Effect of Injection Parameters and Swirl on Diesel Combustion Eith Figh Pressure Fuel Injection," *SAE* 910489.

Kato, T., Tujimura, K., Shintani, M., Minami, T. and Yamaguchi, I., 1989, "Spray Characteristics and Combustion Improvement of D. I. Diesel Engine with High Pressure Fuel Injection," *SAE* 890265.

Kato, T., Koyama, T., Sasaki, K., Koji Mori and Kazutoshi Mori, 1998, "Common Rail Fuel Injection System for Improvement of Engine Performance on Heavy Duty Diesel Engine," *SAE* 980806.

Watkins, A. P., 1989, "Three-Dimensional Modelling of Gas Flow and Sprays in Diesel Engines," In Markatos, N. C., editor, *Computer Simulation of Fluid Flow, Heat and Mass Transfer and Combustion in Reciprocating Engines*, pp. 193~237.

Spalding, D. B., 1980, "A General Computer Program for Fluid-Flow, Heat Transfer and Chemical Reaction Processes," Int. FEM-Congress.

Araki, K. and Moriyama, A., 1982, "Deformation Behaviour of a Liquid Droplet Impinging on a Hot Metal Surface," *In Int. Cont. on Liquid Atomization and Spraying Systems* ICLASS-82.

Jayaratne, O. W. and Mason, B. T., 1964, "The Coalescence and Bouncing of Water Drop at Air/

Water Interface," *Proc. R. Soc.* Lond-A 280, p. 545.

Wachters, L. H. J. and Westerling, N. A. J., 1966, "The Heat Transfer from a Hot Wall to Impinging Water Drops in the Spheroidal State," *Chemical Engineering Science*, 21, p. 1047.

Arcoumanis, C. and Chang, J. C., 1994, "Flow and Heat Transfer Characteristics of Impinging Transient Diesel Sprays," *SAE* 940678.

Naber, J. D. and Farrell, P., 1993, "Hydrodynamics of Droplet Impingement on a Heated Surface," *SAE* 930919.

Park, K. and Watkins,A. P., 1996, "Assessement and Application of A New Spray wall Impaction Model," *Computers in Reciprocating Engines and Gas Turbines, IMechE*, pp. 1~10.

Suzuki, M., Nishida, K. and Hiroyasu, H., 1993, "Simultaneous Concentration Measurement of Vapour and Liquid in An Evaporating Diesel Spray," *SAE* 930863.

Reitz, R. D. and Diwakar, R., 1986, "Effect of Drop Breakup on Fuel Sprays," *SAE* 860469.